Geophysical Research Letters

RESEARCH LETTER
10.1029/2022GL100379

Key Points:

- Samples in diamond anvil cell experiments contract and expand in a strongly non-isotropic fashion upon compression and decompression
- Experimental reports on iron conductivity at high pressure contain errors due to the assumption of isotropic contraction or expansion
- Accurate in situ determination of sample geometry is necessary for thermal and electrical conductivity measurements at high pressure

Supporting Information:

Supporting Information may be found in the online version of this article.

Correspondence to:

S. S. Lobanov and Z. M. Geballe,
slobanov@gfz-potsdam.de;
zgeballe@carnegiescience.edu

Citation:

Lobanov, S. S., & Geballe, Z. M. (2022). Non-isotropic contraction and expansion of samples in diamond anvil cells: Implications for thermal conductivity at the core-mantle boundary. *Geophysical Research Letters*, *49*, e2022GL100379. https://doi.org/10.1029/2022GL100379

Received 8 JUL 2022
Accepted 21 SEP 2022

Non-Isotropic Contraction and Expansion of Samples in Diamond Anvil Cells: Implications for Thermal Conductivity at the Core-Mantle Boundary

Sergey S. Lobanov[1] and Zachary M. Geballe[2]

[1]Deutsches GeoForschungsZentrum GFZ, Potsdam, Germany, [2]Earth and Planets Laboratory, Carnegie Institution of Washington, Washington, DC, USA

Abstract The thermal conductivities of mantle and core materials have a major impact on planetary evolution, but their experimental determination requires precise knowledge of sample thickness at high pressure. Despite its importance, thickness in most diamond anvil cell (DAC) experiments is not measured but inferred from equations of state, assuming isotropic contraction upon compression or assuming isotropic expansion upon decompression. Here we provide evidence that in DAC experiments both assumptions are invalid for a range of mechanically diverse materials (KCl, NaCl, Ar, MgO, silica glass, Al_2O_3). Upon compression, these samples are ~30–50% thinner than expected from isotropic contraction. Most surprisingly, all the studied samples continue to thin upon decompression to 10–20 GPa. Our results partially explain some discrepancies among the highly controversial thermal conductivity values of iron at Earth's core conditions. More generally, we suggest that *in situ* characterization of sample geometry is essential for conductivity measurements at high pressure.

Plain Language Summary The thermal and electrical conductivities of the materials making up Earth's core and lowermost mantle are crucial inputs for modeling Earth's interior and the geodynamo mechanism. Yet, large disagreements between published values of conductivity are common, including a factor-of-seven discrepancy in the thermal conductivity of iron at core-mantle boundary conditions. One possible source of systematic uncertainty is the estimate of sample thickness during high-pressure experiments. Here we show that common materials in compression experiments tend to thin by much more than previously assumed. Surprisingly, the thinning continues upon decompression. These thinning trends could lead to ~30–50% systematic error, partially explaining the discrepancy in iron conductivity. *In situ* thickness measurements are thus crucial for accurate determination of conductivities of Earth's mantle and core.

1. Introduction

The cooling rate of the core is controlled by the thermal conductivity of the mantle at the core-mantle boundary (CMB) (Lay et al., 2008). A thermally-stratified outermost core develops if the mantle is not able to remove the heat supplied by conduction at the top of the core (Lister & Buffett, 1998; Mound et al., 2019). This is a plausible scenario given the extant data on the thermal conductivities of the mantle and core materials (Williams, 2018). Crystallization of the inner core leaves lower density elements in the liquid, causing compositional buoyancy to be a major driver of present-day core convection (Driscoll & Du, 2019). Prior to inner core nucleation, however, it is less clear whether thermal or compositional convection alone could have driven the geodynamo (Davies, 2015; Du et al., 2019; Pozzo et al., 2012). And yet Earth's paleomagnetic record is much older (at least 3.4 Gy (Tarduno et al., 2010; Tarduno et al., 2020)) than current estimates of inner core age (~1 Gy (Bono et al., 2019; Davies, 2015; Driscoll & Bercovici, 2014; Pozzo et al., 2012)), so some combination of buoyancies certainly drove dynamo action. The plausibility of thermally driven convection in the core prior to inner core nucleation depends on many factors, notably thermal conductivity of iron alloys (Davies, 2015; Driscoll & Bercovici, 2014; Landeau et al., 2022). Recent experimental reports on the thermal conductivity of iron at the CMB differ by nearly a factor of seven, ranging from 33 to 226 W/m/K (Gomi et al., 2013; Konopkova et al., 2016; Ohta et al., 2016; Zhang et al., 2020). The source of this large discrepancy has not been identified.

High-pressure experiments in diamond anvil cells (DACs) allow measurements of thermal conductivity at CMB conditions, but accurate knowledge of the sample thickness is crucial in these experiments (Zhou et al., 2022). Despite their importance, the thicknesses of samples are almost never measured *in*

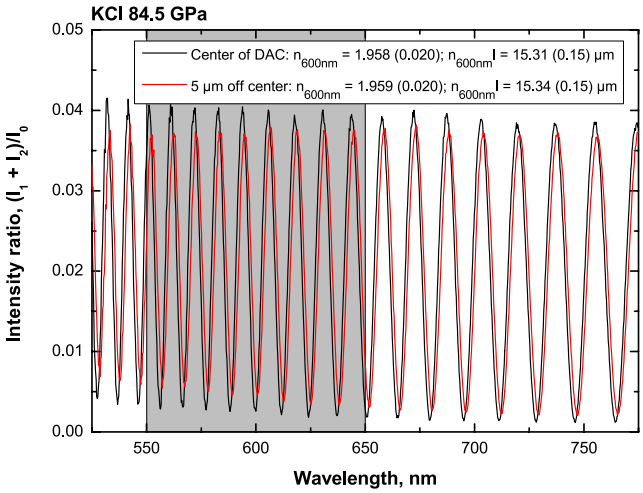

Figure 1. Intensity ratio spectra ($(I_1 + I_2)/I_0$) measured in KCl at 84.5 GPa at the center of the diamond anvil cell (DAC) cavity and ∼5 μm off the center. See Lobanov et al. (2022) for graphical definitions of the measured quantities. The gray box depicts the spectral range used for averaging the signal to obtain the refractive index at 600 nm (n_{600nm}). The different contrast of the two fringe patterns is due to diamond cupping (van Straaten & Silvera, 1988), which apparently has no effect on the inferred refractive index. The optical path length ($n_{600nm}l$) is ∼30 nm longer when measured off center from the axis of the diamond anvils. This is not a significant source of error in sample thickness.

situ in DACs. Instead, the thickness of each sample at high pressure, l, is commonly inferred from the measured thickness prior to the experiment (Zhang et al., 2020) or after decompression (Geballe et al., 2020; Gomi et al., 2013), assuming isotropic contraction upon compression or isotropic expansion upon decompression: $l/l_0 = (V/V_0)^{1/3}$, where V_0 and V are the unit cell volumes at 1 atm and high pressure given by the room temperature equation of state. In this study, we employ direct optical measurements of the thickness of samples in DAC experiments and find that it evolves in a strongly non-isotropic fashion for a mechanically diverse set of samples. Using our measurements to correct the results of previous studies for non-isotropic behavior, we find that the discrepancy in iron conductivities is indeed smaller than the discrepancy without our correction. *In situ* measurements of sample thickness are thus crucial for accurate future measurements of thermal conductivity in DACs.

2. Materials and Methods

The flat tips of diamond anvils form an interferometer; thus, the distance between the anvils can be measured directly by analyzing the interference pattern in the spectrum of a reflected (or transmitted) white light if the refractive index of the sample is known (Dewaele et al., 2003; Kim et al., 2021). Here we apply a recently developed approach (Lobanov et al., 2022) to measure the diamond-to-diamond separation upon compression up to ∼135 GPa (P at the CMB) and subsequent decompression. Briefly, our approach involves reflecting a broadband laser probe from the diamond-sample-diamond assemblage and recording the reflected signal on a charge-coupled device. The ratio of incoming (I_0) and reflected ($I_1 + I_2$) intensities (Figure 1) averaged over 550–650 nm allows finding the refractive index at 600 nm (n_{600nm}). The sample thickness (l) is then obtained from the spectral separation of the observed extrema which yields the optical path length ($n_{600nm}l$) under the assumption that index dispersion in the measured spectral range is small. The overall uncertainty in l is ∼1% (Lobanov et al., 2022).

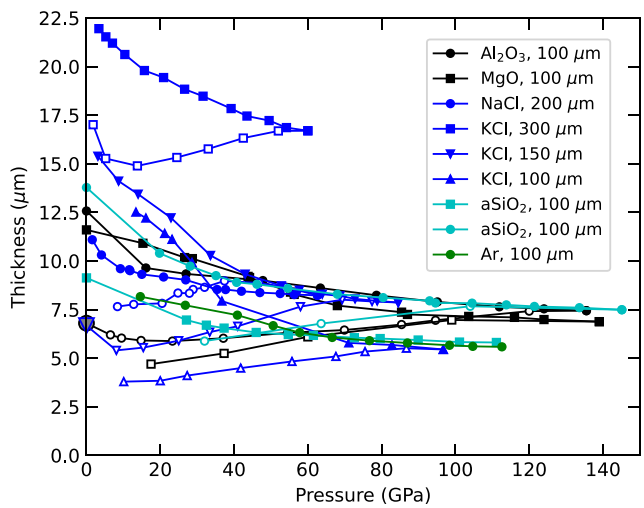

Figure 2. Diamond-diamond distance (sample thickness) in diamond anvil cell experiments with Al_2O_3, MgO, NaCl, KCl, Ar, and silica glass ($aSiO_2$) as samples on compression (solid symbols) and decompression (hollow symbols). Gray shading inside symbols marks the thicknesses of fully decompressed samples measured with an SEM. The legend also indicates the diamond culet diameter. The uncertainty in sample thickness is ∼1%.

We prepared sample chambers by indenting 250 μm thick rhenium foils between 300 or 200 μm flat anvils or 300/150 μm or 300/100 μm beveled anvils and subsequently laser-drilling holes with diameters of ∼100 or ∼35 μm at the center of the indentation. The sample chambers were filled entirely with either SiO_2 glass ($aSiO_2$), Al_2O_3, MgO, KCl, NaCl, or Ar. These are common pressure media used in DAC experiments, and they have diverse mechanical properties ranging from highly incompressible Al_2O_3 (K_0 = 255 GPa (Oganov & Ono, 2005)) to highly compressible Ar (K_0 ∼ 2.65 GPa (Dewaele et al., 2021)). The bulk moduli of B1 and B2 NaCl and KCl are intermediate (K_0 ∼ 20–30 GPa (Dewaele et al., 2012; Dorogokupets & Dewaele, 2007)) while $aSiO_2$ is relatively compressible in the pressure range 0–40 GPa but more incompressible at pressures above 40 GPa (Petitgirard et al., 2017). Refractive indices of these materials will be reported elsewhere. Pressure was measured by the diamond Raman edge method with the relative uncertainty of ±5% (for 300/150 and 300/100 μm bevel/culet diameters) (Akahama & Kawamura, 2004) and by the spectral position of the ruby R1 line (for 200 and 300 μm culet diameters) (Syassen, 2008). The thicknesses of several fully decompressed samples were measured by cutting through the gaskets with a focused ion beam (FIB) and directly imaging the thickness in a scanning electron microscope (SEM).

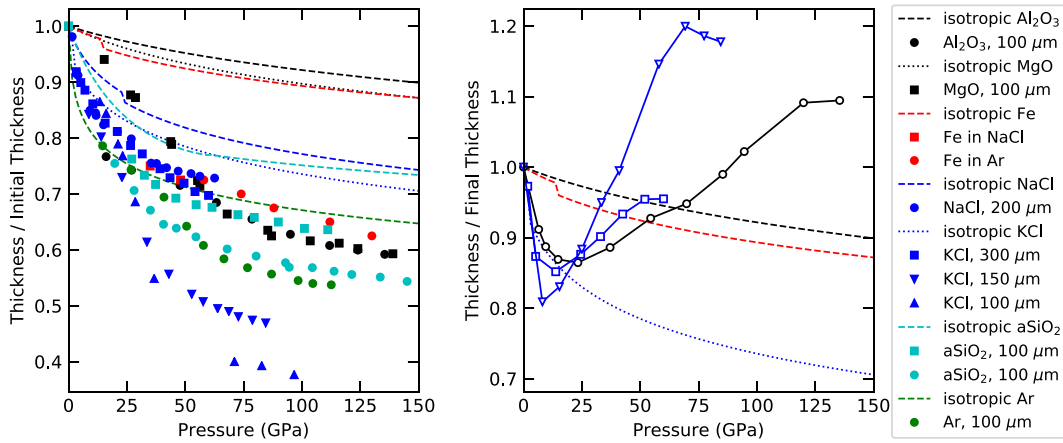

Figure 3. Diamond-diamond distance (sample thickness) normalized to its pre-compression value (LEFT) and after full decompression (RIGHT) as compared to models of isotropic contraction and expansion, following the equations of state in Refs. (Dewaele & Torrent, 2013; Dewaele et al., 2006, 2012; Petitgirard et al., 2017; Speziale et al., 2001). The thicknesses of Fe in NaCl and Ar media are from Konopkova et al. (2016).

3. Results

All absolute sample thicknesses recorded upon compression (solid symbols) and decompression (open symbols) are shown in Figure 2. Regardless of the sample, its thickness upon compression is always smaller than calculated assuming isotropic contraction (Figure 3 LEFT), likely due to uniaxial stress conditions in the sample cavity: $\sigma_{axial} > \sigma_{radial}$. The decrease in normalized thicknesses upon compression to ~100 GPa is larger for relatively compressible materials (*e.g.*, KCl, Ar) than for incompressible ones (*e.g.*, Al_2O_3, MgO) (Figure 3 LEFT). This observation indicates that the thinning upon compression is material-dependent. However, other experimental parameters also affect the evolution of sample thickness. Notably, the diamond culet diameter, the starting gasket thickness, the initial sample chamber diameter, and the sample packing ratio (initial volume of sample/volume of sample chamber). The effect of diamond culet diameter is clear in the relative thickness data for KCl: smaller culets result in greater thinning (Figure 3 LEFT). For a fixed sample and culet diameter, the normalized thicknesses upon compression is reproducible within ~10% (see $aSiO_2$, 100 μm culets). Upon decompression, isotropic expansion would predict that all samples thicken. Surprisingly, all samples in this study thin upon decompression from the highest pressure down to ~10–20 GPa. Upon final decompression from ~10 GPa to ambient pressure, all samples thicken, consistent with direct thickness measurements by SEM/FIB in select fully decompressed samples. These decompression trends are similar to that noted in helium by Dewaele et al. (2003). Sample thinning upon decompression is also evident from the radial stretching of the gasket holes filled with Al_2O_3 (300/100 μm bevel/culet diameter) or KCl (300/150 μm bevel/culet diameter). In the case of Al_2O_3, the radial stretching upon decompression from 135.5 to 9.5 GPa is 33%, while the expected isotropic expansion is only 8% (Figure S1 TOP in Supporting Information S1). Similarly, decompressing KCl from 84.5 to 8 GPa results in a radial expansion of 40%, whereas the expected isotropic expansion is 16% (Figure S2 TOP in Supporting Information S1). Possible reasons for thinning upon decompression are related to forces at the gasket-diamond interface. The observed outward flow of the sample upon decompression could be triggered by the release of stresses on gasket material near the edge of the culet, due to elastic relaxation of the "cupped" diamond culet (Hemley et al., 1997). In addition, a decrease in static friction between diamond and gasket could allow sample material to flow along the diamond-gasket interface, as suggested by the observation of the recovered gasket-sample assemblage (Figure S1 BOTTOM in Supporting Information S1).

4. Discussion

Previous DAC studies of iron conductivity at 135 GPa relied on the assumption of isotropic contraction/expansion of iron samples upon compression/decompression in Al_2O_3 (Gomi et al., 2013) and $aSiO_2$ (Zhang et al., 2020) pressure media. The adequacy of this assumption depends on the extent to which the deformation of iron is affected by the uniaxial stresses developed in the pressure media. Because the yield strength of iron

is smaller than that of Al_2O_3 and of $aSiO_2$ (Dong et al., 2014; Gleason & Mao, 2013; Hemley et al., 1997; Lacroix et al., 2012; Mao et al., 2008; Singh et al., 1998; Wakabayashi et al., 2015), we assume the linear strain of iron in each dimension is equal to the linear strain of Al_2O_3 or $aSiO_2$, and refer to this as the "matching strains assumption" hereafter. When iron is compressed in a pressure medium with lower yield strength, one might expect thickness variations that are relatively close to the isotropic model, at least compared to compression of iron in Al_2O_3 or $aSiO_2$. Yet, direct thickness measurements by white-light interferometry reported by Konopkova et al. (2016) show that iron samples in NaCl and Ar media thin by ~25–38% upon compression to 35–130 GPa, whereas the expected isotropic thinning is only 5%–12%. (Figure 3 LEFT). These data show that the thinning of iron samples is nearly as great as that of NaCl and Ar (despite their relatively low yield strengths). We surmise, therefore, that the "matching strains assumption" may represent the maximum yet common departure from the isotropic thinning model, even for samples in relatively soft pressure media.

These observations motivate us to use our data on the variation of thicknesses of Al_2O_3 and $aSiO_2$ upon compression and decompression to approximate the error in the thickness estimates of iron samples at 135 GPa caused by the assumption of its isotropic contraction and expansion. Non-isotropic contraction of $aSiO_2$ to 135 GPa results in 45% thinning in our experiments, whereas the isotropic model for iron used in Zhang et al. (2020) predicts a mere 12% thinning (Figure 3 LEFT). Decompression of alumina from 135 GPa results in 9% thinning in our experiments, whereas the isotropic model for iron used in Gomi et al. (2013) predicts a 9% thickening (Figure 3 RIGHT). These discrepancies, combined with the matching strains assumption, suggest that systematic errors of several tens of percent may be present in the inferred values of conductivity in previous studies.

For metals, thermal conductivity (k) is related to electrical resistivity (ρ) through the Wiedemann-Franz Law:

$$k = \frac{1}{\rho} LT \tag{1}$$

where L is the Lorentz number and T is temperature. In the experiments of Zhang et al. (2020) and Gomi et al. (2013) the resistivity of iron samples is calculated by:

$$\rho = \rho_0 \frac{R}{R_0} \frac{l}{l_0} \tag{2}$$

where ρ_0 is the resistivity at ambient pressure, R_0 (R) and l_0 (l) are resistances and thickness at ambient (high) pressure. Combining this equation with the Wiedemann-Franz Law yields the proportionality, $k \propto \rho^{-1} \propto l_0/l$. Our results suggest that the models of isotropic contraction and expansion underestimate l_0/l and k in experiments where l_0 is measured prior to compression, but overestimate l_0/l and k in experiments where l_0 is measured after decompression.

Following this logic, we now estimate thickness-related errors in k reported by Zhang et al. (2020) and Ohta et al. (2016). Note that here we correct the high-temperature values reported by Ohta et al. (2016) who used the room-temperature conductivities of Gomi et al. (2013) for normalization. Assuming the errors in estimated sample thicknesses at 135 GPa discussed above, we obtain the following corrections to the thermal conductivity of iron at the pressure and temperature conditions near the CMB: 100 → 133 W/m/K (+33%) for Zhang et al. (2020) and 226 → 185 W/m/K (−18%) for Ohta et al. (2016). The proposed corrections bring the experimental values closer together, and closer to the computed conductivities of iron at similar pressure-temperature conditions from the studies of de Koker et al. (2012) and Pozzo et al. (2012). However, more recent computations of the thermal conductivity of hcp-Fe at CMB conditions that consider electron-electron and electron-phonon scattering point toward a lower value of ~100 W/m/K (Xu et al., 2018). Importantly, the proposed corrections are merely estimates, because the details of pressure-dependent changes in sample thickness depend on many factors, including the relative yield strength of sample versus pressure medium, the strength and compressibility of the gasket material, the shape and size of electrodes, and the gasket's starting thickness and hole diameter. In addition, samples may irreversibly thin at the laser-heated spot due to the release of stresses. Nonetheless, these corrections demonstrate that the controversy in the thermal conductivity of iron at CMB conditions may be partially reconciled by the revised estimates of sample thickness. Although the thicknesses of iron samples have been measured by white-light interferometry at high pressure in Konopkova et al. (2016), the low values of thermal conductivity of iron (33 W/m/K at the CMB) could be systematically biased due to complex, irreversible variations in samples thickness induced by laser heating.

More generally, a word of caution is in order for many other reports on thermal and electrical conductivity at high pressure. The electrical conductivities of Fe-Si-Ni alloys at CMB conditions reported in Refs. (Zhang et al., 2021, 2022) likely need an upward revision because of the assumption of isotropic contraction. Sample thickness at high pressure is also essential for the experimental techniques that determine lattice thermal conductivity in DACs. In these experiments the inferred values of thermal conductivity, k, depend on estimates of sample thickness, l, with an analytical relationship that can be described by $k \propto l^n$ with $n \geq 1.5$. Yagi et al. (2011) proposed $n = 2$ for the thermoreflectance method, which has subsequently been used to study lattice thermal conductivity of lower mantle minerals (Ohta et al., 2012; Okuda et al., 2017, 2020; Yagi et al., 2011). For the laser flash method, Geballe et al. (2020) suggests that $n = 1.5$. Similarly, the inferred thickness of ~100 nm-thick metallic films at high pressure is a crucial parameter for accurate determination of k during time-domain thermoreflectance measurements (Chen et al., 2011). *In situ* measurements of the thickness of these films could be important to test the model of thickness changes during compression used in such studies (Chen et al., 2011; Hsieh et al., 2017, 2018, 2020; Marzotto et al., 2020). Likewise, *in situ* measurement of thickness of metal films on substrates could be important to test the isotropic model of thickness change assumed in picosecond acoustics experiments (Decremps et al., 2014; Edmund et al., 2020). Sample thickness is also essential for the spectroscopic determination of optical absorption coefficients, which serve as primary input for estimates of radiative thermal conductivity (Goncharov et al., 2006, 2008, 2015; Keppler et al., 2008; Lobanov et al., 2017, 2020, 2021; Murakami et al., 2014, 2022; Thomas et al., 2012). Deviations from isotropic contraction and expansion may partially account for the large discrepancy in the estimates of radiative conductivity at the base of the mantle (~0.5–5 W/m/K). Nonetheless, further direct optical measurements of sample thickness in strong and weak pressure media are needed to test the isotropic contraction/expansion assumption and the matching strains assumption.

In closing, we demonstrated that samples contract and expand in a strongly non-isotropic way in DACs for a range of mechanically diverse samples. In all cases, the decrease in thickness is anomalously large upon both compression and decompression. Future measurements of mantle and core thermal conductivity will need to quantify sample thickness at high pressure.

Data Availability Statement

The data set used in this work is deposited at Mendeley Data, V4 (https://doi.org/10.17632/wnvbty8y83.4).

Acknowledgments
S. S. L. acknowledges the support of the Helmholtz Young Investigators Group CLEAR (VH-NG-1325). Z. M. G. acknowledges the support of the National Science Foundation under Grant No. EAR-2125954. We thank Anja Schreiber for technical assistance as well as Sergio Speziale, Jing Yang, and Enrico Marzotto for fruitful discussions and their comments on earlier versions of this manuscript. We are also grateful to the two anonymous reviewers whose suggestions were very helpful. Open access funding enabled and organized by Projekt DEAL.

References

Akahama, Y., & Kawamura, H. (2004). High-pressure Raman spectroscopy of diamond anvils to 250 GPa: Method for pressure determination in the multimegabar pressure range. *Journal of Applied Physics*, *96*(7), 3748–3751. https://doi.org/10.1063/1.1778482

Bono, R. K., Tarduno, J. A., Nimmo, F., & Cottrell, R. D. (2019). Young inner core inferred from Ediacaran ultra-low geomagnetic field intensity. *Nature Geoscience*, *12*(2), 143–147. https://doi.org/10.1038/s41561-018-0288-0

Chen, B., Hsieh, W. P., Cahill, D. G., Trinkle, D. R., & Li, J. (2011). Thermal conductivity of compressed H_2O to 22 GPa: A test of the Leibfried-Schlomann equation. *Physical Review B*, *83*(13), 132301. https://doi.org/10.1103/physrevb.83.132301

Davies, C. J. (2015). Cooling history of Earth's core with high thermal conductivity. *Physics of the Earth and Planetary Interiors*, *247*, 65–79. https://doi.org/10.1016/j.pepi.2015.03.007

Decremps, F., Antonangeli, D., Gauthier, M., Ayrinhac, S., Morand, M., Le Marchand, G., et al. (2014). Sound velocity of iron up to 152 GPa by picosecond acoustics in diamond anvil cell. *Geophysical Research Letters*, *41*(5), 1459–1464. https://doi.org/10.1002/2013gl058859

de Koker, N., Steinle-Neumann, G., & Vlcek, V. (2012). Electrical resistivity and thermal conductivity of liquid Fe alloys at high P and T, and heat flux in Earth's core. *Proceedings of the National Academy of Sciences of the United States of America*, *109*(11), 4070–4073. https://doi.org/10.1073/pnas.1111841109

Dewaele, A., Belonoshko, A. B., Garbarino, G., Occelli, F., Bouvier, P., Hanfland, M., & Mezouar, M. (2012). High-pressure high-temperature equation of state of KCl and KBr. *Physical Review B*, *85*(21), 214105. https://doi.org/10.1103/physrevb.85.214105

Dewaele, A., Eggert, J. H., Loubeyre, P., & Le Toullec, R. (2003). Measurement of refractive index and equation of state in dense He, H_2, H_2O, and Ne under high pressure in a diamond anvil cell. *Physical Review B*, *67*(9), 094112. https://doi.org/10.1103/physrevb.67.094112

Dewaele, A., Loubeyre, P., Occelli, F., Mezouar, M., Dorogokupets, P. I., & Torrent, M. (2006). Quasihydrostatic equation of state of iron above 2 Mbar. *Physical Review Letters*, *97*(21), 215504. https://doi.org/10.1103/physrevlett.97.215504

Dewaele, A., Rosa, A. D., Guignot, N., Andrault, D., Rodrigues, J. E. F. S., & Garbarino, G. (2021). Stability and equation of state of face-centered cubic and hexagonal close packed phases of argon under pressure. *Scientific Reports*, *11*(1), 15192. https://doi.org/10.1038/s41598-021-93995-y

Dewaele, A., & Torrent, M. (2013). Equation of state of alpha-Al_2O_3. *Physical Review B*, *88*(6), 064107. https://doi.org/10.1103/physrevb.88.064107

Dong, H., Dorfman, S. M., Wang, J., He, D., & Duffy, T. S. (2014). The strength of ruby from X-ray diffraction under non-hydrostatic compression to 68 GPa. *Physics and Chemistry of Minerals*, *41*(7), 527–535. https://doi.org/10.1007/s00269-014-0664-2

Dorogokupets, P. I., & Dewaele, A. (2007). Equations of state of MgO, au, pt, NaCl-B1, and NaCl-B2: Internally consistent high-temperature pressure scales. *High Pressure Research*, *27*(4), 431–446. https://doi.org/10.1080/08957950701659700

Driscoll, P. E., & Bercovici, D. (2014). On the thermal and magnetic histories of Earth and Venus: Influences of melting, radioactivity, and conductivity. *Physics of the Earth and Planetary Interiors*, *236*, 36–51. https://doi.org/10.1016/j.pepi.2014.08.004

Driscoll, P. E., & Du, Z. X. (2019). Geodynamo conductivity limits. *Geophysical Research Letters*, *46*(14), 7982–7989. https://doi.org/10.1029/2019gl082915

Du, Z. X., Boujibar, A., Driscoll, P., & Fei, Y. W. (2019). Experimental constraints on an MgO Exsolution-driven geodynamo. *Geophysical Research Letters*, *46*(13), 7379–7385. https://doi.org/10.1029/2019gl083017

Edmund, E., Gauthier, M., Antonangeli, D., Ayrinhac, S., Boccato, S., Deletang, T., et al. (2020). Picosecond acoustics technique to measure the sound velocities of Fe-Si Alloys and Si single-crystals at high pressure. *Minerals*, *10*(3), 214. https://doi.org/10.3390/min10030214

Geballe, Z. M., Sime, N., Badro, J., van Keken, P. E., & Goncharov, A. F. (2020). Thermal conductivity near the bottom of the Earth's lower mantle: Measurements of pyrolite up to 120 GPa and 2500 K. *Earth and Planetary Science Letters*, *536*, 116161. https://doi.org/10.1016/j.epsl.2020.116161

Gleason, A. E., & Mao, W. L. (2013). Strength of iron at core pressures and evidence for a weak Earth's inner core. *Nature Geoscience*, *6*(7), 571–574. https://doi.org/10.1038/ngeo1808

Gomi, H., Ohta, K., Hirose, K., Labrosse, S., Caracas, R., Verstraete, M. J., & Hernlund, J. W. (2013). The high conductivity of iron and thermal evolution of the Earth's core. *Physics of the Earth and Planetary Interiors*, *224*, 88–103. https://doi.org/10.1016/j.pepi.2013.07.010

Goncharov, A. F., Haugen, B. D., Struzhkin, V. V., Beck, P., & Jacobsen, S. D. (2008). Radiative conductivity in the Earth's lower mantle. *Nature*, *456*(7219), 231–234. https://doi.org/10.1038/nature07412

Goncharov, A. F., Lobanov, S. S., Tan, X., Hohensee, G. T., Cahill, D. G., Lin, J. F., et al. (2015). Experimental study of thermal conductivity at high pressures: Implications for the deep Earth's interior. *Physics of the Earth and Planetary Interiors*, *247*, 11–16. https://doi.org/10.1016/j.pepi.2015.02.004

Goncharov, A. F., Struzhkin, V. V., & Jacobsen, S. D. (2006). Reduced radiative conductivity of low-spin (Mg, Fe)O in the lower mantle. *Science*, *312*(5777), 1205–1208. https://doi.org/10.1126/science.1125622

Hemley, R. J., Mao, H. K., Shen, G. Y., Badro, J., Gillet, P., Hanfland, M., & Hausermann, D. (1997). X-ray imaging of stress and strain of diamond, iron, and tungsten at megabar pressures. *Science*, *276*(5316), 1242–1245. https://doi.org/10.1126/science.276.5316.1242

Hsieh, W. P., Deschamps, F., Okuchi, T., & Lin, J. F. (2017). Reduced lattice thermal conductivity of Fe-bearing bridgmanite in Earth's deep mantle. *Journal of Geophysical Research: Solid Earth*, *122*(7), 4900–4917. https://doi.org/10.1002/2017jb014339

Hsieh, W. P., Deschamps, F., Okuchi, T., & Lin, J. F. (2018). Effects of iron on the lattice thermal conductivity of Earth's deep mantle and implications for mantle dynamics. *Proceedings of the National Academy of Sciences of the United States of America*, *115*(16), 4099–4104. https://doi.org/10.1073/pnas.1718557115

Hsieh, W. P., Goncharov, A. F., Labrosse, S., Holtgrewe, N., Lobanov, S. S., Chuvashova, I., et al. (2020). Low thermal conductivity of iron-silicon alloys at Earth's core conditions with implications for the geodynamo. *Nature Communications*, *11*(1), 3332. https://doi.org/10.1038/s41467-020-17106-7

Keppler, H., Dubrovinsky, L. S., Narygina, O., & Kantor, I. (2008). Optical absorption and radiative thermal conductivity of silicate perovskite to 125 Gigapascals. *Science*, *322*(5907), 1529–1532. https://doi.org/10.1126/science.1164609

Kim, Y. J., Celliers, P. M., Eggert, J. H., Lazicki, A., & Millot, M. (2021). Interferometric measurements of refractive index and dispersion at high pressure. *Scientific Reports*, *11*(1), 12853. https://doi.org/10.1038/s41598-021-84883-6

Konopkova, Z., McWilliams, R. S., Gomez-Perez, N., & Goncharov, A. F. (2016). Direct measurement of thermal conductivity in solid iron at planetary core conditions. *Nature*, *534*(7605), 99–101. https://doi.org/10.1038/nature18009

Lacroix, R., Kermouche, G., Teisseire, J., & Barthel, E. (2012). Plastic deformation and residual stresses in amorphous silica pillars under uniaxial loading. *Acta Materialia*, *60*(15), 5555–5566. https://doi.org/10.1016/j.actamat.2012.07.016

Landeau, M., Fournier, A., Nataf, H.-C., Cébron, D., & Schaeffer, N. (2022). *Sustaining Earth's magnetic dynamo*. Nature Reviews Earth & Environment.

Lay, T., Hernlund, J., & Buffett, B. A. (2008). Core-mantle boundary heat flow. *Nature Geoscience*, *1*(1), 25–32. https://doi.org/10.1038/ngeo.2007.44

Lister, J. R., & Buffett, B. A. (1998). Stratification of the outer core at the core-mantle boundary. *Physics of the Earth and Planetary Interiors*, *105*(1–2), 5–19. https://doi.org/10.1016/s0031-9201(97)00082-4

Lobanov, S. S., Holtgrewe, N., Ito, G., Badro, J., Piet, H., Nabiei, F., et al. (2020). Blocked radiative heat transport in the hot pyrolitic lower mantle. *Earth and Planetary Science Letters*, *537*, 116176. https://doi.org/10.1016/j.epsl.2020.116176

Lobanov, S. S., Holtgrewe, N., Lin, J. F., & Goncharov, A. F. (2017). Radiative conductivity and abundance of post-perovskite in the lowermost mantle. *Earth and Planetary Science Letters*, *479*, 43–49. https://doi.org/10.1016/j.epsl.2017.09.016

Lobanov, S. S., Soubiran, F., Holtgrewe, N., Badro, J., Lin, J.-F., & Goncharov, A. F. (2021). Contrasting opacity of bridgmanite and ferropericlase in the lowermost mantle: Implications to radiative and electrical conductivity. *Earth and Planetary Science Letters*, *562*, 116871. https://doi.org/10.1016/j.epsl.2021.116871

Lobanov, S. S., Speziale, S., Winkler, B., Milman, V., Refson, K., & Schifferle, L. (2022). Electronic, structural, and mechanical properties of SiO_2 glass at high pressure inferred from its refractive index. *Physical Review Letters*, *128*(7), 077403. https://doi.org/10.1103/physrevlett.128.077403

Mao, W. L., Struzhkin, V. V., Baron, A. Q., Tsutsui, S., Tommaseo, C. E., Wenk, H. R., et al. (2008). Experimental determination of the elasticity of iron at high pressure. *Journal of Geophysical Research: Solid Earth*, *113*(B9). https://doi.org/10.1029/2007JB005229

Marzotto, E., Hsieh, W. P., Ishii, T., Chao, K. H., Golabek, G. J., Thielmann, M., & Ohtani, E. (2020). Effect of water on lattice thermal conductivity of ringwoodite and its implications for the thermal evolution of descending slabs. *Geophysical Research Letters*, *47*(13), e2020GL087607. https://doi.org/10.1029/2020gl087607

Mound, J., Davies, C., Rost, S., & Aurnou, J. (2019). Regional stratification at the top of Earth's core due to core-mantle boundary heat flux variations. *Nature Geoscience*, *12*(7), 575. https://doi.org/10.1038/s41561-019-0381-z

Murakami, M., Goncharov, A. F., Hirao, N., Masuda, R., Mitsui, T., Thomas, S. M., & Bina, C. R. (2014). High-pressure radiative conductivity of dense silicate glasses with potential implications for dark magmas. *Nature Communications*, *5*(1), 5428. https://doi.org/10.1038/ncomms6428

Murakami, M., Goncharov, A. F., Miyajima, N., Yamazaki, D., & Holtgrewe, N. (2022). Radiative thermal conductivity of single-crystal bridgmanite at the core-mantle boundary with implications for thermal evolution of the Earth. *Earth and Planetary Science Letters*, *578*, 117329. https://doi.org/10.1016/j.epsl.2021.117329

Oganov, A. R., & Ono, S. (2005). The high-pressure phase of alumina and implications for Earth's D" layer. *Proceedings of the National Academy of Sciences of the United States of America*, *102*(31), 10828–10831. https://doi.org/10.1073/pnas.0501800102

Ohta, K., Kuwayama, Y., Hirose, K., Shimizu, K., & Ohishi, Y. (2016). Experimental determination of the electrical resistivity of iron at Earth's core conditions. *Nature*, *534*(7605), 95–98. https://doi.org/10.1038/nature17957

Ohta, K., Yagi, T., Taketoshi, N., Hirose, K., Kornabayashi, T., Baba, T., et al. (2012). Lattice thermal conductivity of $MgSiO_3$ perovskite and post-perovskite at the core-mantle boundary. *Earth and Planetary Science Letters*, *349*, 109–115. https://doi.org/10.1016/j.epsl.2012.06.043

Okuda, Y., Ohta, K., Hasegawa, A., Yagi, T., Hirose, K., Kawaguchi, S. I., & Ohishi, Y. (2020). Thermal conductivity of Fe-bearing post-perovskite in the Earth's lowermost mantle. *Earth and Planetary Science Letters*, *547*, 116466. https://doi.org/10.1016/j.epsl.2020.116466

Okuda, Y., Ohta, K., Yagi, T., Sinmyo, R., Wakamatsu, T., Hirose, K., & Ohishi, Y. (2017). The effect of iron and aluminum incorporation on lattice thermal conductivity of bridgmanite at the Earth's lower mantle. *Earth and Planetary Science Letters*, *474*, 25–31. https://doi.org/10.1016/j.epsl.2017.06.022

Petitgirard, S., Malfait, W. J., Journaux, B., Collings, I. E., Jennings, E. S., Blanchard, I., et al. (2017). SiO_2 glass density to lower-mantle pressures. *Physical Review Letters*, *119*(21), 215701. https://doi.org/10.1103/physrevlett.119.215701

Pozzo, M., Davies, C., Gubbins, D., & Alfe, D. (2012). Thermal and electrical conductivity of iron at Earth's core conditions. *Nature*, *485*(7398), 355–358. https://doi.org/10.1038/nature11031

Singh, A. K., Mao, H. K., Shu, J., & Hemley, R. J. (1998). Estimation of single-crystal elastic moduli from polycrystalline X-ray diffraction at high pressure: Application to FeO and iron. *Physical Review Letters*, *80*(10), 2157.

Speziale, S., Zha, C. S., Duffy, T. S., Hemley, R. J., & Mao, H. K. (2001). Quasi-hydrostatic compression of magnesium oxide to 52 GPa: Implications for the pressure-volume-temperature equation of state. *Journal of Geophysical Research: Solid Earth*, *106*(B1), 515–528. https://doi.org/10.1029/2000jb900318

Syassen, K. (2008). Ruby under pressure. *High Pressure Research*, *28*(2), 75–126. https://doi.org/10.1080/08957950802235640

Tarduno, J. A., Cottrell, R. D., Bono, R. K., Oda, H., Davis, W. J., Fayek, M., et al. (2020). Paleomagnetism indicates that primary magnetite in zircon records a strong Hadean geodynamo. *Proceedings of the National Academy of Sciences of the United States of America*, *117*(5), 2309–2318. https://doi.org/10.1073/pnas.1916553117

Tarduno, J. A., Cottrell, R. D., Watkeys, M. K., Hofmann, A., Doubrovine, P. V., Mamajek, E. E., et al. (2010). Geodynamo, solar wind, and magnetopause 3.4 to 3.45 billion years ago. *Science*, *327*(5970), 1238–1240. https://doi.org/10.1126/science.1183445

Thomas, S. M., Bina, C. R., Jacobsen, S. D., & Goncharov, A. F. (2012). Radiative heat transfer in a hydrous mantle transition zone. *Earth and Planetary Science Letters*, *357*, 130–136. https://doi.org/10.1016/j.epsl.2012.09.035

van Straaten, J., & Silvera, I. F. (1988). Equation of state of solid molecular H_2 and D_2 at 5 K. *Physical Review B*, *37*(4), 1989–2000. https://doi.org/10.1103/physrevb.37.1989

Wakabayashi, D., Funamori, N., & Sato, T. (2015). Enhanced plasticity of silica glass at high pressure. *Physical Review B*, *91*(1), 014106. https://doi.org/10.1103/PhysRevB.91.014106

Williams, Q. (2018). The thermal conductivity of Earth's core: A key geophysical parameter's constraints and uncertainties. *Annual Review of Earth and Planetary Sciences*, *46*(1), 47–66. https://doi.org/10.1146/annurev-earth-082517-010154

Xu, J. Q., Zhang, P., Haule, K., Minar, J., Wimmer, S., Ebert, H., & Cohen, R. E. (2018). Thermal conductivity and electrical resistivity of solid iron at Earth's core conditions from first principles. *Physical Review Letters*, *121*(9), 096601. https://doi.org/10.1103/physrevlett.121.096601

Yagi, T., Ohta, K., Kobayashi, K., Taketoshi, N., Hirose, K., & Baba, T. (2011). Thermal diffusivity measurement in a diamond anvil cell using a light pulse thermoreflectance technique. *Measurement Science and Technology*, *22*(2), 024011. https://doi.org/10.1088/0957-0233/22/2/024011

Zhang, Y. J., Hou, M. Q., Driscoll, P., Salke, N. P., Liu, J., Greenberg, E., et al. (2021). Transport properties of Fe-Ni-Si alloys at Earth's core conditions: Insight into the viability of thermal and compositional convection. *Earth and Planetary Science Letters*, *553*, 116614. https://doi.org/10.1016/j.epsl.2020.116614

Zhang, Y. J., Hou, M. Q., Liu, G. T., Zhang, C. W., Prakapenka, V. B., Greenberg, E., et al. (2020). Reconciliation of experiments and theory on transport properties of iron and the geodynamo. *Physical Review Letters*, *125*(7), 078501. https://doi.org/10.1103/physrevlett.125.078501

Zhang, Y. J., Luo, K., Hou, M. Q., Driscoll, P., Salke, N. P., Minar, J., et al. (2022). Thermal conductivity of Fe-Si alloys and thermal stratification in Earth's core. *Proceedings of the National Academy of Sciences of the United States of America*, *119*(1). https://doi.org/10.1073/pnas.2119001119

Zhou, Y., Dong, Z. Y., Hsieh, W. P., Goncharov, A. F., & Chen, X. J. (2022). Thermal conductivity of materials under pressure. *Nature Reviews Physics*, *4*(5), 319–335. https://doi.org/10.1038/s42254-022-00423-9